# Discrete-time Sliding Mode Observer for the state estimation of a manoeuvring target

Journal Title
XX(X):1–8

DOI: 10.1177/ToBeAssigned
www.sagepub.com/
SAGE

**K. Harikumar [1], Titas Bera [2], Rajarshi Bardhan [3], and Suresh Sundaram [4]**

**Abstract**

This paper addresses the problem of estimating the position, velocity, and acceleration of a manoeuvring target from noisy position measurements. A discrete-time sliding mode observer (DSMO) is designed to handle unmeasured disturbance input and measurement noise. A first order linear dynamics is considered for target acceleration. The acceleration input command and the pole of the first order acceleration dynamics are considered to be unknown parameters with known upper bounds. A finite non-zero boundary layer is employed to reduce the chattering phenomenon typically associated with sliding mode observers. Analysis of estimation error dynamics is presented for the case where the DSMO is operating outside the boundary layer and also within the boundary layer. An algorithm is developed for obtaining the observer gain vector that guarantees the stability of the error dynamics. Numerical simulations and experimental results are presented to validate the stability and performance of the proposed observer.

**Keywords**

Discrete-time sliding mode observer, Error dynamics, Polytopic uncertainty, Target tracking.

## Introduction

Tracking a moving object or a manoeuvring target vehicle is highly important in the area of missile guidance, surveillance, etc (1). The efficiency of various target tracking algorithms is highly dependent on the availability of the accurate position, velocity, and acceleration information of the target. If a sensor like a camera or LIDAR is used, then the approximate position information of the target can be obtained (2). In practice, the sensors used to obtain the target state information is prone to measurement errors. Moreover, most of the sensors cannot measure all the states (position, velocity, and acceleration) of the target under consideration. So a state estimator or an observer is required to determine the accurate target state information from the noisy sensor measurements.

Interacting multiple model (IMM) method is used for the state estimation of manoeuvring targets in (3)-(5). The IMM method based state estimation uses multiple interacting state estimators and fuses their output to get the target state estimate (5). But IMM method based state estimation is computationally intensive as multiple state estimators need to be executed in parallel. Another popular algorithm for target state estimation is Kalman filter (6)-(8). Kalman filter is the optimal estimator for linear systems driven by disturbances and measurement noise follows a Gaussian probability distribution (9). The target acceleration is considered as the disturbance input in state estimation. But the Gaussian nature of target acceleration cannot be guaranteed for all the cases. So a computationally efficient method of state estimation, capable of handling non-Gaussian disturbances and measurement noise is required.

Sliding mode observers are popular due to their robustness with respect to model uncertainties (10). They can also handle unmeasured disturbances with known upper bound (11). Discrete-time sliding mode observers (DSMO) are preferred for systems with measurements available at finite sampling time (12). The applications of DSMO can be found in areas like chemical, electrical and satellite technology (13)-(15). A DSMO is developed in this paper for the state estimation of a manoeuvring target. Noisy position information of the target is used to estimate accurate position, velocity, and acceleration of the target. The upper bounds on the target acceleration input command and measurement noise are assumed to be known.

The main contributions of this paper are as follows. Unlike the DSMO design mentioned in the above literature, the present paper incorporates measurement noise explicitly in the observer design. A finite non-zero boundary layer is used to reduce chattering. The stabilization of estimation error dynamics leads to the stabilization problem of a linear system with polytopic uncertainty. An algorithm

[1]Computational Intelligence Lab, School of Computer Science and Engineering, Nanyang Technological University Singapore, 639798. email: kharikumar@ntu.edu.sg, harikumar100@gmail.com.
[2] TCS Innovation Labs, Kolkata, India, 700156. email: titas1979@gmail.com.
[3] ST Engineering-NTU Corporate Laboratory, School of Electrical and Electronic Engineering, Nanyang Technological University Singapore, 639798. email: rbardhan@ntu.edu.sg.
[4] Department of Aerospace Engineering, Indian Institute of Science, Bangalore, India, 560012. email: sureshsundaram@iisc.ac.in.

**Corresponding author:**
K. Harikumar, Computational Intelligence Lab, School of Computer Science and Engineering, Nanyang Technological University Singapore, 639798. kharikumar@ntu.edu.sg, harikumar100@gmail.com.
**Funding**: The research work was fully funded by the ST Engineering - NTU Corporate Laboratory, Singapore, under the project CRP3-P2P.

is proposed to compute the observer gain vector that guarantees the stability of the estimation error dynamics in the presence of uncertain target acceleration input command and measurement noises. A preliminary version of this paper is available in (16). The preliminary version discusses the structure of the DSMO with a simulation result and experimental result for the estimation of target position and velocity. The current paper proposes an algorithm to obtain the observer gains that guarantees the stability of estimation error dynamics within and outside of the boundary layer. The algorithm uses the genetic algorithm (GA) to minimize a performance index to obtain the observer gain vector. Detailed simulation results are presented for a sinusoidally manoeuvring target showing the performance of the proposed DSMO for a different amplitude of target manoeuvres. The proposed DSMO is also compared with other two state of the art robust discrete-time observers and found to perform better at higher measurement noise amplitudes. Experimental results are given for the estimation of position, velocity, and acceleration of a sinusoidally manoeuvring target. Both simulation and experimental results indicate that the proposed DSMO has stable estimation error dynamics.

The paper is organized as follows. The target dynamics and state estimation problem is introduced in the section titled "Problem Formulation." The structure of DSMO and algorithm for obtaining observer gain vector is presented in the section titled "Discrete-time Sliding Mode Observer." Observer gain vector synthesis and simulated state estimation results are presented in the section titled "Simulation results for observer gain synthesis and target state estimation." Experimental results are given in the section titled "Experimental results for state estimation." The paper is concluded in the section titled "Conclusion."

## Problem formulation

This section formulates the state estimation problem and explains the target dynamics. The target assumed here is a ground vehicle manoeuvring along the inertial $XY$ plane. The dynamics of the target along $X$-axis and $Y$-axis is treated independently as any constraint on minimum turn radius is not imposed. Therefore, the state estimation problem along $X$-axis is only discussed in this paper. The same formulation and analysis are applicable for state estimation along the $Y$-axis. A first order model is adopted to represent the acceleration dynamics of the target. Let the position, velocity, and acceleration of the target along $X$-axis is denoted by $p_x$, $v_x$ and $a_x$ respectively. Then, the target dynamics along the $X$-axis is given below (17).

$$\dot{\bar{X}} = A\bar{X} + B\bar{U} \tag{1}$$

where $\bar{X} = [p_x \ v_x \ a_x]^T$ and $U = a_{xin}$ is the input acceleration command of the target. The input $a_{xin}$ is bounded by a known positive constant, ie. $|a_{xin}| <= a_m \ \forall \ t > 0$. The system matrix $A$ is given by,

$$A = \begin{pmatrix} 0 & 1 & 0 \\ 0 & 0 & 1 \\ 0 & 0 & p_a \end{pmatrix} \tag{2}$$

where $p_a < 0$ is the pole of first order acceleration dynamics and is an unknown parameter with a known bound denoted by $p_{am}$, i.e. $|p_a| <= p_{am}$ where $p_{am} > 0$. The input matrix $B$ is given below.

$$B = \begin{pmatrix} 0 \\ 0 \\ -p_a \end{pmatrix} \tag{3}$$

The position information added with noise is the measurement available to estimate the target states. The output equation is given by,

$$Y = C\bar{X} + \eta \tag{4}$$

The output matrix in the above equation is given below where $\eta$ denotes the measurement noise.

$$C = [1, \ 0, \ 0] \tag{5}$$

The position measurement is obtained at a fixed time interval of $T$ seconds. A discrete time state space model of the target dynamics that is used in formulating the observer dynamics is derived as given below.
The target dynamics given in (1) is partitioned into a known dynamics part and an unknown dynamics part as given below.

$$\dot{\bar{X}} = A_1\bar{X} + A_2\bar{X} + B\bar{U} \tag{6}$$

Here, the known matrix is $A_1$ and the unknown matrices are $A_2$ and $B$. The known matrix,

$$A_1 = \begin{pmatrix} 0 & 1 & 0 \\ 0 & 0 & 1 \\ 0 & 0 & 0 \end{pmatrix} \tag{7}$$

and the unknown matrix

$$A_2 = \begin{pmatrix} 0 & 0 & 0 \\ 0 & 0 & 0 \\ 0 & 0 & p_a \end{pmatrix} \tag{8}$$

Target dynamics given in (6) is further represented as

$$\dot{\bar{X}} = A_1\bar{X} + D \tag{9}$$

where $D = A_2\bar{X} + B\bar{U}$ is the unknown disturbance input given by

$$D = \begin{pmatrix} 0 \\ 0 \\ p_a a_x - p_a a_{xin} \end{pmatrix} \tag{10}$$

The discrete time representation of state equation given in (9) and output equation given in (4) is shown in (11) and (12) respectively.

$$\bar{X}([k+1]T) = A_{1d}\bar{X}(kT) + D_d(kT) \tag{11}$$

$$Y(kT) = C_d\bar{X}(kT) + \eta_d(kT) \tag{12}$$

where $T$ is the sampling time, $k$ is an integer. The state vector, $\bar{X}(k) = [p_x(kT), \ v_x(kT), \ a_x(kT)]^T$, $D(kT)$ is the unmeasured disturbance input and $\eta_d(kT)$ is the measurement noise. The maximum absolute value of $\eta_d(kT)$, denoted by $\eta_m$ is assumed to be known. The system

matrix $A_{1d}$ is given by,

$$A_{1d} = \begin{pmatrix} 1 & T & 0.5T^2 \\ 0 & 1 & T \\ 0 & 0 & 1 \end{pmatrix} \quad (13)$$

Let the maximum absolute values of the elements of $D(kT)$ are denoted by $d_{1m}$, $d_{2m}$ and $d_{3m}$. Then it can be shown that,

$$D_m = \begin{pmatrix} d_{1m} \\ d_{2m} \\ d_{3m} \end{pmatrix} = a_m p_{am} \begin{pmatrix} \frac{T^3}{3} \\ T^2 \\ 2T \end{pmatrix} \quad (14)$$

The output matrix $C_d$ is same as the matrix $C$ given in (5). The discrete time system model given in (11) to (14) is obtained using the state space response equation given below.

$$X(T) = e^{A_1 T} X(0) + \int_0^T e^{A_1(T-\tau)} D(\tau) d\tau \quad (15)$$

The objective is to estimate the unknown state vector, $\bar{X}(k) = [p_x(kT),\ v_x(kT),\ a_x(kT)]^T$ of the target using the output equation given by (12). The construction of DSMO is discussed in the following section. For convenience, the discrete time instant is represented as $k$ instead of $kT$ in the rest of the paper (i.e. the sampling time $T$ is not explicitly mentioned in the rest of the equations).

## Discrete-time sliding mode observer

The DSMO dynamics is given below (12).

$$\hat{X}(k+1) = A_{1d}\hat{X}(k) + L(Y(k) - C_d\hat{X}(k)) + \beta(k) \quad (16)$$

In the above equation, it can be verified that the pair $(A_{1d}, C_d)$ is observable. The observer gain is denoted by the vector $L$ and $\beta(k)$ is the saturation function given by,

$$\beta(k) = R\ sat(\frac{Y(k) - C_d\hat{X}(k)}{\gamma}) \quad (17)$$

where $R = [r_1,\ r_2,\ r_3]^T$ with $r_1 > 0$, $r_2 > 0$, $r_3 > 0$. The scalar parameter $\gamma > 0$ and

$$sat(y) = \begin{cases} y, if(|y| \leq 1) \\ sign(y), if(|y| > 1) \end{cases} \quad (18)$$

Let the measurement residual be denoted by $Q(k)$ as given below.

$$Q(k) = Y(k) - C_d\hat{X}(k) \quad (19)$$

The DSMO dynamics is inside the boundary layer for $|Q(k)| <= \gamma$ and outside the boundary layer otherwise. The estimation error, denoted by $e(k)$ is given below.

$$e(k) = \bar{X}(k) - \hat{X}(k) \quad (20)$$

The analysis of error dynamics outside the boundary layer ($|Q(k)| > \gamma$) is presented in the next subsection, followed by the analysis of error dynamics inside the boundary layer ($|Q(k)| <= \gamma$).

### *Error dynamics outside the boundary layer*

The error dynamics given below can be derived using (11), (12) and (16).

$$e(k+1) = [A_{1d} - LC_d]e(k) + [D_d(k) - L\eta_d(k)] - \beta(k) \quad (21)$$

***Lemma 1***: For $|Q(k)| > \gamma$, there exists a vector $P(k)$, where $0 < P(k) < \frac{2R}{\gamma}$ such that

$$[D_d(k) - L\eta_d(k)] - \beta(k) = -P(k)Q(k) \quad (22)$$

***Proof***: For $|Q(k)| > \gamma$, it is evident that $\beta(k) = \pm R$ from (17). By choosing the elements of $R$ such that $R > D_m + |Ln_m|$, it is evident that the absolute value of the elements of $[D_d(k) - L\eta_d(k)] - \beta(k)$ lies between $(0,\ 2R)$. So for $|Q(k)| > \gamma$, $P(k)$ lies between $(0,\ \frac{2R}{\gamma})$.
Using (22) and (19), the error dynamics given in (21) can be rewritten as below.

$$e(k+1) = [A_{1d} - LC_d - P(k)C_d]e(k) - P(k)\eta_d(k) \quad (23)$$

Let

$$A_c = [A_{1d} - LC_d - P(k)C_d] \quad (24)$$

If $A_c$ has its eigenvalues inside a unit circle $\forall k > 0$, then the estimation error is bounded (as $P(k)$ and $\eta_d(k)$ are bounded). The choice of $L$ determines the stability of $A_c$ with unknown bounded vector $P(k)$. The observer gain $L$ is obtained as described below.
Let $L = [l_1,\ l_2,\ l_3]^T$ and

$$R = \begin{pmatrix} r_1 \\ r_2 \\ r_3 \end{pmatrix} = \begin{pmatrix} d_{1m} + |l_1 n_m| + \delta_1 \\ d_{2m} + |l_2 n_m| + \delta_2 \\ d_{3m} + |l_3 n_m| + \delta_3 \end{pmatrix} \quad (25)$$

Here $\delta_1,\ \delta_2,\ \delta_3 > 0$. The choice of $R$ given in (25) ensures that the condition $R > D_m + |Ln_m|$ mentioned in the proof of *Lemma 1* is satisfied. It can be easily verified that the matrix $A_c$ is having polytopic uncertainty. The system dynamics given in (21) is stable if the matrix $A_c$ has its eigenvalues within a unit circle for all the vertices of the polytope (18). From (24), (25) and noting that $P(k)$ lies between $(0,\ \frac{2R}{\gamma})$, the vertices of polytope can be obtained. The vertices of the polytope are given by $v_1 = [l_1,\ l_2,\ l_3]$, $v_2 = [l_1,\ l_2,\ l_3 + \frac{2r_3}{\gamma}]$, $v_3 = [l_1,\ l_2 + \frac{2r_2}{\gamma},\ l_3 + \frac{2r_3}{\gamma}]$, $v_4 = [l_1,\ l_2 + \frac{2r_2}{\gamma},\ l_3]$, $v_5 = [l_1 + \frac{2r_1}{\gamma},\ l_2,\ l_3]$, $v_6 = [l_1 + \frac{2r_1}{\gamma},\ l_2,\ l_3 + \frac{2r_3}{\gamma}]$, $v_7 = [l_1 + \frac{2r_1}{\gamma},\ l_2 + \frac{2r_2}{\gamma},\ l_3 + \frac{2r_3}{\gamma}]$ and $v_8 = [l_1 + \frac{2r_1}{\gamma},\ l_2 + \frac{2r_2}{\gamma},\ l_3]$. Let $A_c(v_i)$ denote the system matrix given in (24), corresponding to the vertex $v_i$, where $i = \{1,\ 2, ..., 8\}$. The observer gain parameters $[l_1,\ l_2,\ l_3]$ are determined using genetic algorithm (GA) as given in the *Algorithm I*.
*Algorithm I*:

---

**STEP I**: Initialize $L = [l_{10},\ l_{20},\ l_{30}]^T$ using any pole-placement technique to place the eigenvalues of $A_c(v_1)$ at a desired location inside the unit circle. Let the desired eigenvalues are denoted by $\lambda_{1d}$, $\lambda_{2d}$ and $\lambda_{3d}$.
**STEP II**: Formulate a performance index $J$ given by

$$J = \sum_{i=1}^{8}\sum_{j=1}^{3} |\lambda_{jd} - \lambda_{ji}| + M \quad (26)$$

where $\lambda_{ji}$ denote the $j^{th}$ eigenvalue of $A_c(v_i)$ and $M$ is a penalty factor accounting for any $|\lambda_{ji}| >= 1$.
**STEP III**: Minimize $J$ defined in STEP II using GA with decision variable $L = [l_1,\ l_2,\ l_3]^T$ with one of the member of initial population of GA as $L = [l_{10},\ l_{20},\ l_{30}]^T$ obtained from STEP I.

---

The *Algorithm I* tries to obtain the observe gains by minimizing the distance of the eigenvalues of the eight matrices $A_c(v_1)....A_c(v_8)$ form the desired eigenvalues $\lambda_{1d}$, $\lambda_{2d}$ and $\lambda_{3d}$. STEP I of *Algorithm I* provides one member of the initial population of GA. The performance index $J$ mentioned in STEP II gives a very high penalty for eigenvalues placed outside the unit circle for any of the matrix $A_c(v_i)$. The observer gains are synthesized in STEP III using GA, by minimizing the performance index mentioned in STEP II.

### *Error dynamics inside the boundary layer*

For $|Q(k)| <= \gamma$, and the error dynamics given below is obtained using (11), (12), (16) and (17).

$$e(k+1) = [A_{1d} - LC_d - \frac{RC_d}{\gamma}]e(k) + F(k) \qquad (27)$$

where

$$F(k) = D_d(k) - L\eta_d(k) - \frac{R\eta_d(k)}{\gamma} \qquad (28)$$

If the matrix $A_c$ given in (24) has its eigenvalues inside the unit circle $\forall k > 0$, then the matrix $[A_{1d} - LC_d - \frac{RC_d}{\gamma}]$ also has its eigenvalues inside the unit circle $\forall k > 0$. So stability of (16) implies the stability of (27). Since $D_d(k)$ and $\eta_d(k)$ is bounded, the disturbance input $F(k)$ in (27) is bounded, resulting in bounded estimation error within the boundary layer.

## Simulation results for observer gain synthesis and target state estimation

Numerical simulations are performed for observer gain synthesis and target state estimation for a sampling time interval of $T = 0.05$ seconds. The maximum acceleration input of the target, $a_m = 2.0$ m/$s^2$ and the maximum absolute value of the pole location, $p_{am} = 4.0$. The other parameters are set at $n_m = 1.0$ and $\delta_1 = \delta_2 = \delta_3 = 0.01$. The desired eigenvalues for initial pole placement is selected as $\lambda_{1d} = 0.30$, $\lambda_{2d} = 0.35$ and $\lambda_{3d} = 0.40$. For $\gamma = 1.0$, the observer gain obtained using *Algorithm I*, for $T = 0.05$ seconds is $L = [0.4106,\ 0.5022,\ 0.0891]^T$. The eigenvalues of the matrices $A_c(v_1)$ to $A_c(v_8)$ are given in Table 1 for $T = 0.05$ seconds, and all of them lies within the unit circle.

In order to analyze the effect of the parameter $\gamma$, observer gains are synthesized using *Algorithm I* for different $\gamma$ values varying from 0.5 to 2.0. The resulting observer gains are given in Table 2. For the different observer gains given in Table 2, a numerical simulation for state estimation is performed with initial conditions $\bar{X}(0) = [10.0, 2.0, 1.0]^T$, $\hat{X}(0) = [8.0, 0.0, 0.0]^T$. The initial conditions are kept same for the simulations carried out in the next two subsections. The input acceleration command of the target, $a_{xin} = A_x cos(\omega t)$ with $A_x = 1.5$, $\omega = 0.2\pi$ and the pole of the target dynamics $p_a = -3.0$. The position of the target is sampled at a time interval of $T = 0.05$ seconds and a random noise generated from uniform probability distribution is added to obtain the measurement for the DSMO. The plots of estimated and true position, velocity and acceleration is given in figures 1, 2 and 3 respectively. The highest initial overshoot in estimation of velocity and acceleration is for $\gamma = 2.0$, and is lowest for $\gamma = 1.0$.

**Table 1.** Eigenvalues of $A_c(v_1)$ to $A_c(v_8)$ for $T$=0.05 seconds.

| $\lambda_1$ | $\lambda_2$ | $\lambda_3$ |
|---|---|---|
| 0.6621 | 0.9379 | 0.9894 |
| 0.6292 | 0.9801 +j 0.1110 | 0.9801 - j0.1110 |
| 0.8406 + j0.1613 | 0.8406 - j0.1613 | 0.9083 |
| 0.7961 + j0.1890 | 0.7961 - j0.1890 | 0.9971 |
| -0.2322 | 0.9898 + j0.0088 | 0.9898 - j0.0088 |
| -0.2333 | 0.9904 + j0.0611 | 0.9904 -j0.0611 |
| -0.1879 | 0.9677 + j0.0541 | 0.9677 - j0.0541 |
| -0.1865 | 0.9370 | 0.9970 |

**Table 2.** Observer gains for different $\gamma$.

| $\gamma$ | $l_1$ | $l_2$ | $l_3$ |
|---|---|---|---|
| 0.5 | 0.3547 | 0.7926 | 0.1658 |
| 1.0 | 0.4106 | 0.5022 | 0.0891 |
| 1.5 | 0.1871 | 0.5176 | 0.1729 |
| 2.0 | 0.2022 | 0.5309 | 0.2841 |

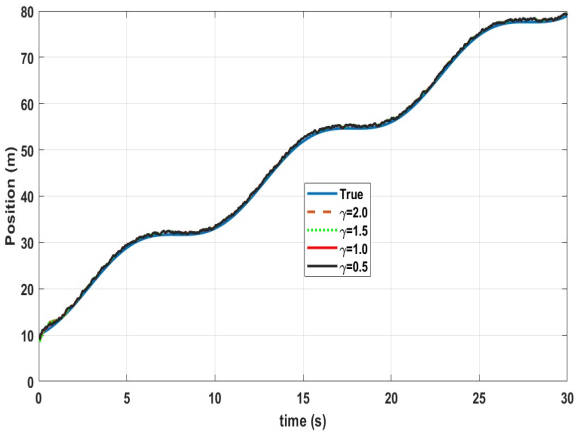


**Figure 1.** True and estimated position for different $\gamma$ values

For comparison, the mean square error (MSE) values in estimation for the position ($E_{p_x}$), velocity ($E_{v_x}$) and acceleration ($E_{a_x}$) estimation is given in Table 3. The MSE value in position estimate is almost the same for all the $\gamma$ values. The MSE values for velocity and acceleration estimate is the lowest for $\gamma = 1.0$. Hence $\gamma = 1.0$ and the corresponding observer gain from Table 2 is used in subsequent sections for further analysis.

The plot of $Q(k)$ for $\gamma = 1$ is given in fig. 4, indicating that the observer dynamics is outside the boundary layer initially and later converges within the boundary layer.

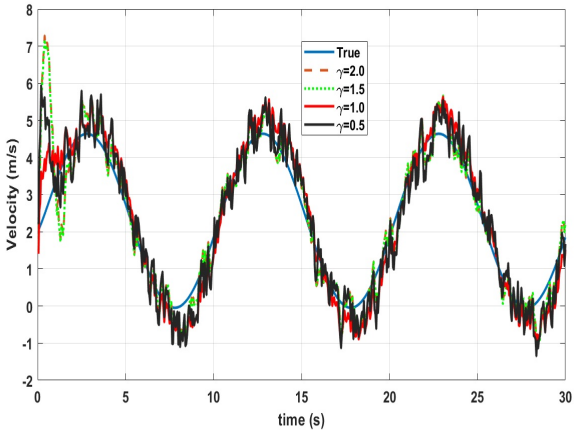


**Figure 2.** True and estimated velocity for different $\gamma$ values

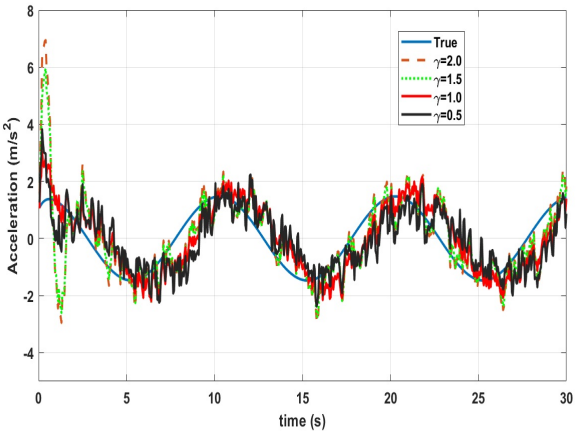


**Figure 3.** True and estimated acceleration for different $\gamma$ values

**Table 3.** MSE values for variation in $\gamma$.

| $\gamma$ | $(E_{p_x})\,(m)$ | $(E_{v_x})\,(m/s)$ | $(E_{a_x})\,(m/s^2)$ |
|---|---|---|---|
| 0.5 | 0.5432 | 0.6708 | 0.9199 |
| 1.0 | 0.5425 | 0.5709 | 0.7460 |
| 1.5 | 0.5408 | 0.7268 | 0.9712 |
| 2.0 | 0.5414 | 0.7402 | 1.0702 |

## *Performance of DSMO for varying target dynamics pole location and input acceleration magnitude*

The performance of the DSMO designed for $a_m = 2.0$ m/$s^2$ and $p_{am} = 4.0$ is further analyzed by varying the amplitude $(A_x)$ of the input acceleration command of the target, $a_{xin} = A_x cos(\omega t)$ and the pole location of the acceleration dynamics $(p_a)$. $A_x$ is varied from 0.5 m/$s^2$ to 2.0 m/$s^2$. The value of $p_a$ is varied from -4.0 to -2.0. The MSE values $E_{p_x}$, $E_{v_x}$ and $E_{a_x}$ are given in Table 4. From Table 4, it is observed that with an increase in $A_x$, the MSE in velocity and acceleration estimation increases. The variation in $p_a$ does not have much effect on the MSE values when compared to variation in $A_x$.

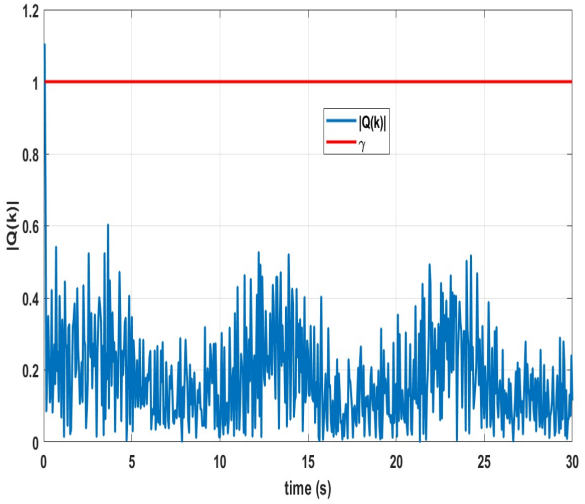


**Figure 4.** Residual for state estimation for $\gamma = 1.0$

**Table 4.** MSE comparison for different target acceleration magnitude and pole location.

| $p_a$ | $A_x$ | $(E_{p_x})\,(m)$ | $(E_{v_x})\,(m/s)$ | $(E_{a_x})\,(m/s^2)$ |
|---|---|---|---|---|
| -4.0 | 0.5 | 0.5430 | 0.3951 | 0.4695 |
| -4.0 | 1.0 | 0.5426 | 0.4630 | 0.5762 |
| -4.0 | 1.5 | 0.5424 | 0.5734 | 0.7483 |
| -4.0 | 2.0 | 0.5429 | 0.7067 | 0.9508 |
| -3.0 | 0.5 | 0.5431 | 0.3927 | 0.4647 |
| -3.0 | 1.0 | 0.5426 | 0.4611 | 0.5742 |
| -3.0 | 1.5 | 0.5425 | 0.5709 | 0.7460 |
| -3.0 | 2.0 | 0.5427 | 0.7029 | 0.9469 |
| -2.0 | 0.5 | 0.5431 | 0.3881 | 0.4562 |
| -2.0 | 1.0 | 0.5428 | 0.4561 | 0.5678 |
| -2.0 | 1.5 | 0.5429 | 0.5630 | 0.7366 |
| -2.0 | 2.0 | 0.5430 | 0.6908 | 0.9319 |

## *Performance comparison with other discrete-time robust observers*

The performance of the proposed DSMO is compared with two other robust estimators, viz. discrete-time Kalman filter (DKF) (9) and discrete-time $H_\infty$ filter (D$H_\infty$F) (19). Simulations are carried out for measurement noise taken from uniform probability distribution with a maximum absolute value of $n_m = \{0.25\,m,\ 0.50\,m,\ ,0.75\,m,\ 1.0\,m\}$. The input acceleration to the target is sinusoidal of the form $a_{xin} = A_x cos(\omega t)$, with the amplitude $A_x = 1.5$ and frequency $\omega = 0.1\pi$. The MSE values $E_{p_x}$, $E_{v_x}$ and $E_{a_x}$ for DSMO, DKF and D$H_\infty$F are given in Table 5. From Table 5, it is inferred that the performance of the DSMO for velocity estimation is better when compared to DKF and D$H_\infty$F at higher noise levels. For the case of acceleration, DSMO gives the best estimate at all noise levels. D$H_\infty$F gives the best estimate of position for all noise levels. The plot for position, velocity and acceleration estimation for $n_m = 0.5\,m$ is given in fig. 5, fig. 6 and fig. 7 respectively. From fig. 7, it is clear that DSMO tracks the target acceleration better when compared to DKF and D$H_\infty$F.

**Table 5.** MSE comparison for different observers with varying noise level.

| Observer | $n_m$ | $(E_{p_x})\,(m)$ | $(E_{v_x})\,(m/s)$ | $(E_{a_x})\,(m/s^2)$ |
|---|---|---|---|---|
| DSMO | 0.25 | 0.1084 | 0.2918 | 0.3672 |
| DKF | 0.25 | 0.2305 | 0.2374 | 0.3827 |
| D$H_\infty$F | 0.25 | 0.0725 | 0.2601 | 0.4303 |
| DSMO | 0.5 | 0.1984 | 0.3595 | 0.4473 |
| DKF | 0.5 | 0.2582 | 0.3576 | 0.5176 |
| D$H_\infty$F | 0.5 | 0.1409 | 0.4368 | 0.6432 |
| DSMO | 0.75 | 0.2917 | 0.4472 | 0.5446 |
| DKF | 0.75 | 0.2950 | 0.4997 | 0.6838 |
| D$H_\infty$F | 0.75 | 0.2103 | 0.6299 | 0.8857 |
| DSMO | 1.0 | 0.3816 | 0.5466 | 0.6520 |
| DKF | 1.0 | 0.3381 | 0.6494 | 0.8635 |
| D$H_\infty$F | 1.0 | 0.2801 | 0.8281 | 1.1391 |

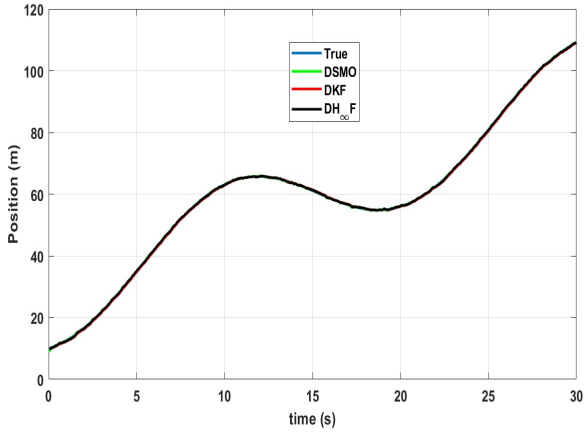


**Figure 5.** Comparison of DSMO with $DKF$ and $DH_\infty F$ for position estimation ($n_m = 0.5\,m$)

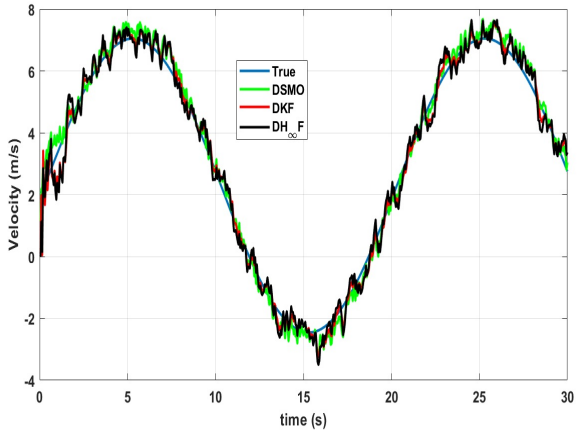


**Figure 6.** Comparison of DSMO with $DKF$ and $DH_\infty F$ for velocity estimation ($n_m = 0.5\,m$)

## Experimental results for state estimation

The experiment is conducted using a remotely operated unmanned ground vehicle (UGV) shown in fig. 8. The maximum acceleration of the UGV is close to 4.0 $m/s^2$. The UGV is equipped with a real time kinematic (RTK) GPS module for position and velocity measurement. The RTK-GPS module gives very accurate inertial position and inertial velocity measurements with respect to a fixed location on

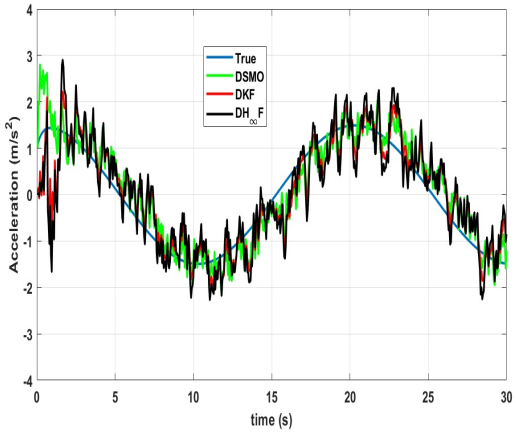


**Figure 7.** Comparison of DSMO with $DKF$ and $DH_\infty F$ for acceleration estimation ($n_m = 0.5\,m$)

the ground where the base station GPS for RTK system is mounted (20). The location of the base station GPS is taken as the origin of the inertial coordinate system with $X$-axis pointing towards the north and $Y$-axis pointing towards the east. A 3-axis accelerometer module is mounted on the UGV to measure the acceleration along the body axis of the UGV. From the RTK velocity measurements, the heading of the UGV is computed. The heading information is used to convert body axis acceleration measurement into inertial axis acceleration measurement. The UGV is remotely operated and follows two circular paths of different radius. Both the RTK-GPS module and accelerometer are interfaced to a Raspberry-Pi computer mounted on the UGV. The data is sampled at an interval of $T$= 0.05 seconds and stored in the memory of the Raspberry-Pi computer. The observer gain is obtained using *Algorithm I*, with the parameters $a_m = 4.0\,m/s^2$ and $p_{am}$=10. Rest all parameters are kept same as mentioned in the previous numerical simulation section. The observer gain vector is given by $L = [0.4620,\ 1.2612,\ 0.0856]^T$.

The initial conditions for the state estimation along the $X$-axis is given by $\bar{X}(0) = [7.484, 0.729, -2.138]^T$ and $\hat{X}(0) = [5.0, 0.0, 0.0]^T$. Random noise generated from uniform probability distribution with a maximum amplitude of 0.5 m is added to the RTK-GPS position values to get noisy position measurement. The RTK position, RTK velocity and accelerometer data is considered as the true states for comparison with estimated states. The plots of true and estimated position, velocity and acceleration are given in figs. 9, 10 and 11 respectively. The plot of residual is given in fig. 12. Similar to the numerical simulation data, the experimental data also indicate that the estimation error dynamics converges into the boundary layer and the estimation error is bounded. The MSE values of state estimate for the experiment is given in Table 6.

**Table 6.** MSE values of state estimation for experiment.

| $(E_{p_x})\,(m)$ | $(E_{v_x})\,(m/s)$ | $(E_{a_x})\,(m/s^2)$ |
|---|---|---|
| 0.265 | 1.347 | 2.390 |

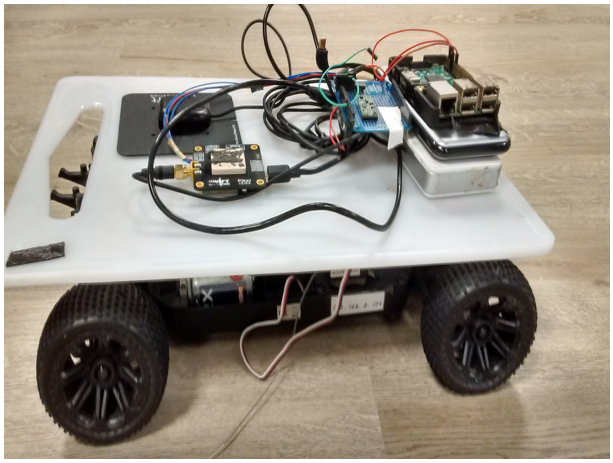

**Figure 8.** Target UGV mounted with RTK-GPS module and accelerometer.

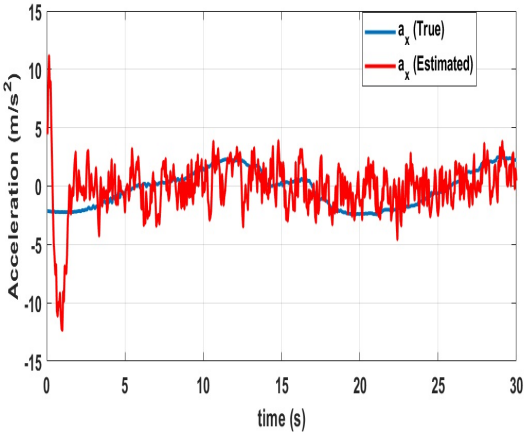


**Figure 11.** Experimental- True and estimated $X$-axis acceleration

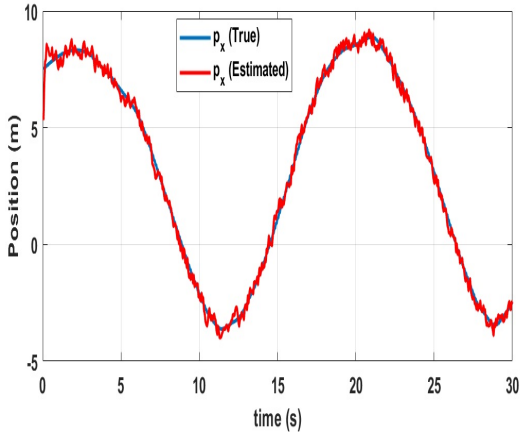


**Figure 9.** Experimental- True and estimated $X$-axis position

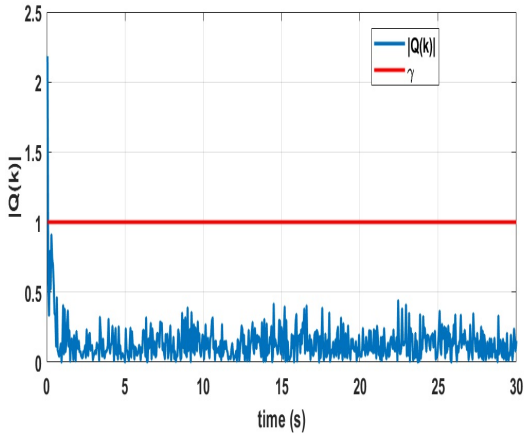


**Figure 12.** Experimental- Residual for state estimation along $X$-axis

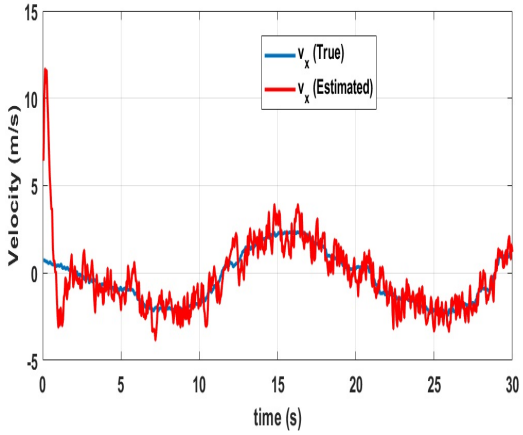


**Figure 10.** Experimental- True and estimated $X$-axis velocity

## Conclusion

This paper addressed the problem of estimating the states of a manoeuvring target from noisy position measurements obtained at a fixed time interval. The discrete-time sliding mode observer (DSMO) design proposed in this paper can handle bounded and unknown target acceleration input and measurement noise. The design of DSMO leads to the stabilization problem of an uncertain polytopic system. The proposed algorithm finds the observer gain vector by minimizing a performance index using the genetic algorithm. Error dynamics is found to stable within and outside the boundary layer. It is observed from simulation results that there is an increase in the mean square error in estimation when the target acceleration magnitude increases. Comparison with two other discrete-time robust observers shows promising results for the proposed DSMO. The performance of the proposed DSMO improves with an increase in noise level when compared to DKF and D$H_\infty$F. Further, simulation and experimental results indicate that the proposed DSMO has stable estimation error dynamics with a bounded estimation error depending on the target input acceleration and measurement noise level.

## Funding

The research work was fully funded by the ST Engineering - NTU Corporate Lab, Singapore, under the project CRP3-P2P.

## Declaration of Conflicting Interests

The authors declare that there is no conflict of interests.

## References


[1] Yanushevsky, RT. Generalized missile guidance laws against manoeuvring targets. *Proceedings of the Institution of Mechanical Engineers, Part I: Journal of Systems and Control Engineering*2007; 221(4): 645 - 651.

[2] Kandath H, Bera T, Bardhan R and Sundaram S. Autonomous Navigation and Sensorless Obstacle Avoidance for UGV with Environment Information from UAV. *Second IEEE International Conference on Robotic Computing (IRC)* Laguna Hills, CA, 2018, pp. 266-269.

[3] Blair WD, Watson GA, and Rice TR. Interacting multiple model filter for tracking maneuvering targets in spherical coordinates. *IEEE Proceedings of Southeastcon*, Williamsburg, VA, 1991, pp. 1055-1059.

[4] Lan J, Li XR, Jilkov VP and Mu C. Second-Order Markov Chain Based Multiple-Model Algorithm for Maneuvering Target Tracking. *IEEE Transactions on Aerospace and Electronic Systems* 2013; 49(1): 3-19.

[5] Mazor E, Averbuch A, Bar-Shalom Y and Dayan J. Interacting multiple model methods in target tracking: a survey. *IEEE Transactions on Aerospace and Electronic Systems* 1998; 34(1): 103-123.

[6] Mehrotra K and Mahapatra PR. A jerk model for tracking highly maneuvering targets. *IEEE Transactions on Aerospace and Electronic Systems* 1997; 33(4): 1094-1105.

[7] Cao Y, Jiang J, Wang S and Fan Y. Tracking methods of high speed strong maneuvering targets in near space. $12^{th}$ *International Conference on Signal Processing (ICSP)*, Hangzhou, 2014, pp. 1885-1889.

[8] Jin B, Jiu B, Su T, Liu H and Liu G. Switched Kalman filter-interacting multiple model algorithm based on optimal autoregressive model for manoeuvring target tracking. *IET Radar, Sonar & Navigation* 2015; 9(2): 199-209.

[9] Simon D. Optimal State Estimation: Kalman, H-infinity and nonlinear approaches, New York:Wiley, 2006.

[10] Spurgeon SK. Sliding mode observers: a survey. *International Journal of Systems Science* 2008; 39(8): 751-764.

[11] Davila J, Fridman L and Levant A. Second-order sliding-mode observer for mechanical systems. *IEEE Transactions on Automatic Control* 2005; 50(11): 1785-1789.

[12] Thein MWL. A discrete time variable structure observer with overlapping boundary layers. *Proceedings of the 2002 American Control Conference*, Anchorage, AK, USA, 2002, pp. 2633-2638.

[13] Mihoub M, Nouri AS and Abdennour RB. A second order discrete sliding mode observer for the variable structure control of a semi-batch reactor. *Control Engineering Practice* 2011; 19(1): 1216-1222.

[14] Bernardes T, Montagner VF, Grundling HA and Pinheiro H. Discrete-Time Sliding Mode Observer for Sensorless Vector Control of Permanent Magnet Synchronous Machine. *IEEE Transactions on Industrial Electronics* 2014; 61(4): 1679-1691.

[15] Pal M and Seetharama Bhat M. Discrete time second order sliding mode observer for uncertain linear multi-output system. *Journal of the Franklin Institute* 2014; 351(4): 2143-2168.

[16] Harikumar K, Bera T, Bardhan R and Sundaram S. State Estimation of an Agile Target using Discrete Sliding Mode Observer. $5^{th}$ *International Conference on Control, Decision and Information Technologies (CoDIT)*, Thessaloniki, Greece, 2018, pp. 75-79.

[17] Sun HM and Lin TL. An adjustable parameter model for tracking a manoeuvring target. *Proceedings of the Institution of Mechanical Engineers, Part I: Journal of Systems and Control Engineering* 2003; 217(4): 275 - 284.

[18] Peaucelle D, Ebihara Y. Robust stability analysis of discrete-time systems with parametric and switching uncertainties. *Proceedings of* $19^{th}$ *world congress of IFAC*, Cape Town, South Africa, 2014, pp. 724-729.

[19] Bizhong X, Zheng Z, Zizhou L, Wei W, Wei S, Yongzhi L and Mingwang w. Strong Tracking of a H-Infinity Filter in Lithium-Ion Battery State of Charge Estimation. *Energies* 2018; 11(6): 1481.

[20] Harikumar K, Bera T, Bardhan R and Sundaram S. Cooperative obstacle avoidance for heterogeneous unmanned systems during search mission. *Encyclopedia with Semantic Computing and Robotic Intelligence* 2018; 2(1): 1850002-1 to 1850002-8.